Solar influence and hydrological variability during the Holocene from a speleothem annual record (Molinos Cave, NE Spain).

Arsenio Muñoz[1], Miguel Bartolomé[1,2], Alicia Muñoz[1], Carlos Sancho[1], Ana Moreno[2], John C. Hellstrom[3], Mª Cinta Osácar[1] and Isabel Cacho[4]

[1] Department of Earth Sciences, University of Zaragoza, C/ Pedro Cerbuna, 12. 50009 Zaragoza, Spain.

[2] Department of Geoenvironmental Processes and Global Change, Pyrenean Institute of Ecology-CSIC, Avda. Montañana 1005. 50059 Zaragoza, Spain.

[3] School of Earth Sciences, University of Melbourne, Parkville, VIC. 3010 Australia.

[4] Department of Stratigraphy, Palaeontology and Marine Geosciences, University of Barcelona, C/Martí Franques s/n. 08028 Barcelona, Spain.

ABSTRACT

We present a multi-proxy approach to reconstructing Holocene climate conditions in northeastern Spain based on an excellent correlation among the lamina thickness, colour parameters and isotope ($\delta^{18}O$ and $\delta^{13}C$) variations recorded in a speleothem. An age model constructed from five U/Th dates and annual lamina counting suggests that the uppermost 14.7 cm of the MO-7 stalagmite grew between 7.2 and 2.5 kyr before present but experienced a growth hiatus from 4.9 to 4.3 kyr. Three spectral analysis methods were applied to 11 time series. The results reveal common solar periodicities on decennial (Gleissberg cycle) and centennial (De Vries-Suess cycle) scales. The onset of Holocene carbonate precipitation in the MO-7 stalagmite appears to be associated with a cold, wet period, whereas the hiatus and the end of growth are related to warm, dry periods. This environmental trend fits well within the regional Holocene climate.

Key words: Holocene, solar cycles, speleothem, multi-proxy, spectral analysis.

INTRODUCTION

Examples of strong coherence between solar variability and climate cycles suggest that solar activity may be responsible for Holocene climatic oscillations (Yu and Ito, 1999; Bond et al., 2001; Neff et al., 2001; Peristykh and Damon, 2003; Schimmelmann et al., 2003; Raspopov et al., 2008; Kokfelt and Muscheler, 2013; Zhang et al., 2013; Soon et al., 2014).

Past solar cyclicity has been studied on different temporal scales through diverse proxies (e.g., tree rings, lacustrine sediments, speleothems). The results from these analyses suggest the occurrence of three main solar cycles on decennial or centennial scales: the 11-yr Schwabe sunspot cycle (Schwabe, 1844), the ~83-yr Gleissberg cycle (Gleissberg, 1939, 1958) and the ~204-yr De Vries-Suess cycle (De Vries, 1958; Suess, 1980). Variations in solar activity have been well documented, particularly in Holocene speleothemic archives, by identifying changes in colour or isotopic composition (Niggemann et al., 2003; Dykoski et al., 2005; Cosford et al., 2008, 2009; Martín-Chivelet et al., 2011) or variations in the thickness of speleothem layers (Qin et al., 1999; Frisia et al., 2003; Muñoz et al., 2009). Nevertheless, information is scarce and discontinuous, which has limited the identification and definition of the corresponding periodicities.

Techniques for palaeoclimatic reconstruction based on stable isotopes ($\delta^{13}C$ and $\delta^{18}O$) and laminated speleothems have been intensely developed over the last 10 years (e.g., McDermott, 2004; Cheng et al., 2006 and Baker et al., 2008). The Iberian Peninsula is a region with very few palaeoclimate studies based on speleothems; notable among these are the works of Domínguez-Villar et al. (2009), Moreno et al. (2010) and Martín-Chivelet et al. (2011) in northern Spain, which inferred multiple climatic variables from $\delta^{13}C$ and $\delta^{18}O$ isotope stalagmite composition. In this paper, we present a palaeoclimatic record from a laminated speleothem that we analyse through a multi-proxy strategy. We construct 11 independent, high-resolution time series for layer thicknesses, colour variations and stable isotope ($\delta^{18}O$ and $\delta^{13}C$) values. The paper (i) analyses the existing periodicities and their relationships to solar cycles through three spectral analysis methods and (ii) reconstructs Holocene climate conditions in northeastern Spain.

GEOLOGICAL SETTING

Molinos Cave lies in limestones of Cenomanian-Turonian age. It is located in the easternmost sector of the Iberian Range, northeastern Spain, at 40°47'N, 0°26'W, at 1040 m a.s.l. (Fig. 1). The cave was declared a Natural Monument in 2006. Geologically, the study area is part of the Cretaceous Maestrazgo Basin.

The climate of the area is a mid-mountain Mediterranean one (Peña et al., 2002). The mean annual temperature ranges between 12 and 13°C, and the annual precipitation, which is mainly concentrated in spring and autumn, averages 500 mm (Fig. 1) but experiences significant interannual variations. Vegetation cover is sparse but includes scrub and supra-Mediterranean oak forest (Millán et al., 1992). The cave, opened to tourism since the 1960s, is 620 m long and is arranged in two interconnected horizontal levels, the upper "Crystal" and lower "Marine" rooms.

METHODOLOGY

The stalagmite MO-7 was collected *in situ* from the lower level (Marine room) of the Molinos Cave. It was halved along its growth axis, and one of the two symmetrical portions was carefully polished. Image analysis techniques were applied to the polished surface and to thin sections of the speleothem. Samples for isotopic composition and U/Th dating were drilled using carbide dental burrs following stratigraphic horizons (Fig. 2).

Colour measurements on the polished surface were taken using an Avaatech Colour Line Scan that produces visual colour images as well as colour data in red, green, blue (RGB) and CIE-L*-a*-b*. The L*a*b* value is a uniform colour scale recommended by the Commission Internationale de l'Eclairge (CIE). L* defines lightness, a* denotes the red/green value and b* the yellow/blue value. The study of the MO-7 stalagmite provides 6 continuous-signal (Weedon, 2003) time series of 2170 values (corresponding to R, G, B, L*, a* and b* colour parameters) with a resolution of 70 microns (Fig. 2).

Chemical preparation and analysis of five U/Th disequilibrium series were performed at the University of Melbourne, Australia following the methodology described in Hellstrom (2003, 2006). Measurements were taken using a MC-ICP-MS (Thermo-Finnegan Neptune). Details of dates, detrital contents, and corrected initial $\delta^{234}U$ ratios are given in Table 1.

Two discrete-signal (according to terminology from Weedon, 2003) time series (a total of 4105 data points) of lamina thickness (light and dark) were measured using WinGeol LAM software (Meyer et al., 2006). The analysis was performed on high-resolution photomicrographs (1.35 microns per pixel) of thin sections obtained from an Olympus SZX7 stereomicroscope equipped with an Olympus DP20-5E digital camera system. Next, a new time series was derived from the sum of light and dark values by assuming that each light-dark doublet represents an annual increment of growth (Fig. 3). Laminae were anchored to the U/Th ages following the methodology described in Domínguez-Villar et al. (2012).

Two continuous-signal time series of isotopic composition ($\delta^{18}O$ and $\delta^{13}C$) were acquired from samples, each with powder mass from 80 to 100 μg, drilled each millimetre along the central growth axis of the MO-7 stalagmite (Fig. 2) using a drill bit 0.5 mm in diameter. Oxygen and carbon stable isotope analyses of calcite were performed using a Thermo Finnigan MAT252 mass spectrometer coupled to a CarboKiel-III carbonate preparation device at the Scientific and Technological Centers at the University of Barcelona. Analytical precision was estimated to be better than 0.03‰ for $\delta^{13}C$ and 0.08‰ for $\delta^{18}O$ by measuring the certified standard NBS-19. Isotope results are reported in standard delta notation relative to Vienna PDB. The resultant time series of isotopic values are shown in Fig. 4.

An age model for the different proxies (L*, a*, b*, R, G, B and isotopes) was built using the StalAge package in R (version 3.0.2) (Scholz and Hoffman, 2011).

Subsequently, we performed a spectral analysis of the internal lamination, colour variations and stable isotope fluctuations. Two Fourier analysis techniques, (i) the Lomb periodogram algorithm for unevenly sampled data (Press et al., 1992) and (ii) the REDFIT module (Schulz and Mudelsee, 2002), and wavelet analysis (Torrence and Compo, 1998), which are included within the PAST software V. 3.01 (Hammer et al., 2001), were applied to the MO-7 stalagmite records to evaluate the nature and character of the cyclicity. The data were automatically detrended prior to analysis. The results obtained from application of different spectral analysis techniques to independent high-resolution time series may be more reliable than those obtained from any one technique or time series.

RESULTS AND DISCUSSION

Age model and annual lamina development

The top (uppermost 14.7 cm) of the MO-7 stalagmite displays a very well-marked, internal, annually laminated structure characterised by transparent and milk-white calcite couplets (Figs. 2 and 5). The laminated structure is made of columnar calcite fabric (Frisia et al., 2000; Frisia and Borsato, 2010; Fairchild and Baker, 2012).

An age model was constructed from five U/Th dates and lamina counting to represent the studied proxy obtained at different resolutions (70 µm for L*, a*, b*, R, G and B, and 1 mm for isotopes). First, following the methodology described in Domínguez-Villar et al. (2012), a 1:1 slope using the five U-Th ages and the number of laminae was constructed (Fig 6a) and, considering the presence of a hiatus identified in thin section, divided into two segments (above and below the growth interruption). Lamina counts were later anchored to U-Th ages within the error bands (Fig. 6b). These counts were used as tie points in the final construction of the age model using StalAge software (Fig. 6c).

The age model indicates that the uppermost 14.7 cm of the MO-7 stalagmite spans the time period 7.2 to 2.5 kyr before present. Considering the time spans registered (7.2-4.9 kyr and 4.3-2.5 kyr, i.e., ~4.1 kyr), the number of laminae (4105 couplets), and the fact that precipitation is mainly concentrated in spring and autumn, the lamination is consistent with a seasonal origin.

Spectral analysis

Two spectral analysis techniques, Fourier and wavelet, were used to analyse the diverse multi-proxy time series made from stalagmite MO-7 (Fig. 7). The results are very similar, considering the different techniques used.

Fourier spectral analysis (Lomb periodogram and REDFIT module) of the R, G, B and L* colour time series (time domain) shows periodicities at 91 yr (~Gleissberg cycle), 170 yr (~De Vries-Suess cycle) and 421 yr (Fig. 8a). Comparison of the power spectra (REDFIT module) with AR(1) models of red noise suggests the existence of a 91-year periodicity with 99% confidence level (Fig. 8b). The Fourier spectral analysis of the a* and b* colour time series do not find evidence of cyclicity at the 99% confidence level using the AR(1) noise model. The 170-yr period is shorter than that of the De Vries-Suess cycle, although Lüdecke et al. (2015) find frequencies for this cycle that differ from the main ~204-year periodicity. They interpret that solar influence is modified by the response of the Earth system and its inherent forcings. Uniform cycles of approximately 400 yr appear in the annual-layer thickness data and grey level proxies of a Hulu Cave stalagmite (Duan et al., 2015). Other periodicities with $p < 0.01$ (Fig. 8a) can be related to centennial cycles of solar origin (Bond et al., 2001; Springer et al., 2008) or may be false positives predicted by a poor model of the power spectrum.

Wavelet analysis of the lamina thickness (couplet) time series (Fig. 9) shows the same periodicities that approximately correspond to the Gleissberg, De Vries-Suess and ~400 yr cycles. Knudsen et al. (2012) noted an intermittent pattern, also visible in figure 9, of the De Vries-Suess cycle in temperatures derived from stalagmites in China, Turkey and the United States.

High-frequency periodicities (Schwabe and Hale cycles) were not found, possibly because the thick stratigraphic series over the cave smooths out or removes small interannual differences that temperature and rainfall transfer to the lamina thickness.

Fourier spectral analysis of the time series derived from the $\delta^{18}O$ and $\delta^{13}C$ isotopic values shows a similar 183-yr periodicity (Fig. 10). This cycle, although also different from the standard 204-yr cycle, can be related to De Vries-Suess solar cycle (Lüdecke et al., 2015).

Palaeoclimatology

The time interval within the Holocene when the MO-7 stalagmite grew is known to have been especially favourable for speleothem (Moreno et al., 2013) and tufa (Peña et al., 2014) formation in northeastern Iberia. Pollen records from nearby lakes (Aranbarri et al., 2014) also suggest a benign climate. Thicker and darker (reflected light) laminations grew during intervals characterised by more negative $\delta^{13}C$ values (Fig. 11), which are interpreted as longer or more intense rainy winter-spring season periods. During these periods, there would have been increased infiltration into the cave as a result of a higher precipitation-evaporation balance in the region (e.g., Genty et al., 2006; Moreno et al., 2010). On a longer timescale, the onset of the MO-7 stalagmite appears to coincide with a wet interval, as evidenced by thicker laminae and $\delta^{13}C$ values averaging -8.5‰, with significant fluctuations. This was followed by a dry period, as evidenced by thinner and lighter laminae and $\delta^{13}C$ values averaging -7.47‰ beginning at 7.2 kyr and extending to at least 4.9 kyr, when the hiatus in the record begins. The upper part of the stalagmite, 4.3 to 2.5 kyr, corresponds to another wet period, where $\delta^{13}C$ values average -8.56‰. The oscillations in $\delta^{18}O$ values from MO-7 stalagmite are small and do not show robust correlations with global temperature records such as Bond events or sunspots cycles. However, an association of wet conditions at the onset of Holocene carbonate precipitation in the MO-7 stalagmite with a cold event defined by Bond et al. (2001) is observed, whereas the hiatus and the end of the growth period are related to warm, dry times (Bond and sunspot curves). An explanation for this association of cold, wet periods throughout the Holocene in a Mediterranean continental climate is related to the expected decrease in evaporation with cooler temperatures and a consequent increase in water availability. This environmental trend fits well within the Holocene climate of the region.

CONCLUSIONS

The age model and spectral analysis through Fourier and wavelet techniques on multi-proxy time series (lamina thickness, colour parameters and stable isotope values) obtained from a speleothem from the Iberian Range in northeastern Spain allow us to draw several conclusions:

- The uppermost section of the MO-7 stalagmite (14.7 cm) grew between 7.2 and 2.5 kyr before present, with a hiatus in growth from ~4.9 to ~4.3 kyr. These dates are given by an age model constructed from 5 U/Th dates and annual lamina counting. The stalagmite comprises 4105 lamina doublets interpreted to be of annual origin.

- Three spectral analysis methods (Lomb periodogram algorithm, REDFIT module and wavelet analysis) were applied to 11 time series obtained from proxies of lamina thickness, colour parameters and stable isotope values. The results reveal common solar periodicities of decennial (~83-yr Gleissberg) and centennial (mainly ~204-yr De Vries-Suess) scales during the mid to late Holocene. These periodicities are unlikely to be artefacts of any single technique, although their peaks do not show well-defined periods, oscillating within a frequency band.

- Considering the Holocene interval of the MO-7 stalagmite, an excellent correlation between lamina thickness, colour parameters and stable isotope values is observed. Thicker and darker laminations grew during intervals characterised by more negative $\delta^{13}C$ values. The small magnitude of oscillations in $\delta^{18}O$ values prevents a clear correlation with temperature variations. The onset of growth in the Holocene of the MO-7 stalagmite appears to be associated with a wet period (cold in Bond curve), whereas the hiatus and the end of growth are related to dry times (warm in Bond curve).

ACKNOWLEDGEMENTS

This study is a contribution to the CTM2013-48639-C2-1-R (OPERA), CGL2009–10455 and HIDROPAST (CGL2010-16376) projects (Spanish Government-European Regional Development Fund), the UZ2014-CIE-04 project (University of Zaragoza), the GA-LC-030/2011 project (Aragón Government-La Caixa) and the E–28 and S-97 research groups (Aragón Government).

REFERENCES

Aranbarri, J., González-Sampériz, P., Valero-Garcés, B., Moreno, A., Gil-Romera, G., Sevilla-Callejo, M., García-Prieto, E., Di Rita, F., Mata, M.P., Morellón, M., Magri, D., Rodríguez-Lázaro, J. and Carrión, J.S., 2014. Rapid climatic changes and resilient vegetation during the Lateglacial and Holocene in a continental region of south-western Europe. *Global and Planetary Change*, **114**, 50-65.

Baker, A., Smith, C., Jex, C., Fairchild, I.J., Genty, D. and Fuller, L., 2008. Annually laminated speleothems: a review. *International Journal of Speleology*, **37**, 193-206.

Bond, G., Kromer, B., Beer, J., Muscheler, R., Evans, M.N., Showers, W., Hoffmann, S., Lotti-Bond, R., Hajdas, I. and Bonani, G., 2001. Persistent solar influence on North Atlantic climate during the Holocene. *Science*, **294**, 2130-2136.

Cheng, H., Edwards, R.L., Wang, Y., Kong, X., Ming, Y., Kelly, M.J., Wang, X., Gallup, C.D. and Liu, W., 2006. A penultimate glacial monsoon record from Hulu Cave and two-phase glacial terminations. *Geology*, **34**, 17-220.

Cheng, H.; Edwards, R.L.; Shen, C.C.; Polyak, V.J.; Asmerom, Y.; Woodhead, J.D.; Hellstrom, J.; Wang, Y.; Kong, X.; Spötl, C.; Wang, X. and Alexander, E.C., 2013. Improvements in ^{230}Th dating, ^{230}Th and ^{234}U half-life values, and U–Th isotopic measurements by multi-collector inductively coupled plasma mass spectrometry. *Earth and Planetary Science Letters,* **371**, 82-91.

Cosford, J., Qing, H., Eglington, B., Mattey, D., Yuan, D., Zhang, M. and Cheng, H., 2008. East Asian monsoon variability since the Mid-Holocene recorded in a high-resolution, absolute-dated aragonite speleothem from eastern China. *Earth and Planetary Science Letters*, **275**, 296–307.

Cosford, J., Qing, H., Mattey, D., Eglington, B. and Zhang, M., 2009. Climatic and local effects on stalagmite $\delta^{13}C$ values at Lianhua Cave, China. *Palaeogeography, Palaeoclimatology, Palaeoecology*, **280**, 235-244.

De Vries, H., 1958. Variation in concentration of radiocarbon with time and location on Earth, *K. Ned. Akad. Van. Wet.-B*, **61**, 94-102.

Domínguez-Villar, D., Fairchild, I.J., Baker, A., Wang, X., Edwards, R.L. and Cheng, H., 2009. Oxygen isotope precipitation anomaly in the North Atlantic region during the 8.2 ka event. *Geology*, **37**, 1095-1098.

Domínguez-Villar, D., Baker, A., Fairchild, I.J. and Edwards, R.L., 2012. A method to anchor floating chronologies in annually laminated speleothems with U–Th dates. *Quaternary Geochronology*, **14**, 57–66.

Duan, F., Wu, J., Wang, Y., Edwards, R.L., Cheng, H., Kong, X. and Zhang, W., 2015. A 3000-yr annually laminated stalagmite record of the Last Glacial Maximum from Hulu Cave, China. *Quaternary Research*, **83**, 360-369.

Dykoski, C.A., Edwards, R.L., Cheng, H., Yuan, D., Cai, Y., Zhang, M., Lin, Y., Qing, J., An, Z. and Revenaugh, J., 2005. A high-resolution, absolute-dated Holocene and deglacial Asian monsoon record from Dongge Cave, China. *Earth and Planetary Science Letters*, **233**, 71-86.

Fairchild, I.J. and Baker, A., 2012. *Speleothem science: from process to past environments*. John Wiley & Sons.

Frisia, S., Borsato, A., Fairchild, I.J. and McDermott, F., 2000. Calcite fabrics, growth mechanisms, and environments of formation in speleothems from the Italian Alps and southwestern Ireland. *Journal of Sedimentary Research*, **70**, 1183-1196.

Frisia, S., Borsato, A., Preto, N. and McDermott, F., 2003. Late Holocene annual growth in three Alpine stalagmites records the influence of solar activity and the North Atlantic Oscillation on winter climate: *Earth and Planetary Science Letters*, **216**, 411-424.

Frisia, S. and Borsato, A., 2010. Karst. *Developments in Sedimentology*, **61**, 269-318.

Genty, D., Blamart, D., Ghaleb, B., Plagnes, V., Causse, C., Bakalowicz, M., Zouari, K., Chkir, N., Hellstrom, J., Wainer, K. and Bourges, F., 2006. Timing and dynamics of the last deglaciation from European and North African $\delta^{13}C$ stalagmite profiles - comparison with Chinese and South Hemisphere stalagmites. *Quaternary Science Reviews*, **25**, 2118-2142.

Gleissberg, W., 1939. A long-periodic Fluctuation of the Sun-spot Numbers. *Observatory*, **62**, 158-159.

Gleissberg, W., 1958. The eighty-year sunspot cycle. *J. Br. Astron. Assoc,* **68**, 148-152.

Hammer, Ø., Harper, D.A.T. and Ryan, P.D., 2001. PAST: Paleontological statistics software package for education and data analysis. *Palaeontologia Electronica*, **4**, 9 pp.

Hellstrom, J., 2003. Rapid and accurate U/Th dating using parallel ion-counting multi-collector ICP-MS. *Journal of Analytical Atomic Spectrometry* **18**, 1346-1351.

Hellstrom, J., 2006. U-Th dating of speleothems with high initial ^{230}Th using stratigraphical constraint. *Quaternary Geochronology* **1**, 289-295.

Knudsen, M.F., Jacobsen, B.H., Riisager, P., Olsen, J. and Seidenkrantz, M.S., 2012. Evidence of Suess solar-cycle bursts in subtropical Holocene speleothem $\delta^{18}O$ records. *The Holocene*, **22**, 597-602.

Kokfelt, U. and Muscheler, R., 2013. Solar forcing of climate during the last millennium recorded in lake sediments from northern Sweden. *The Holocene*, **23**, 447-452.

Lüdecke, H.J., Weiss, C.O. and Hempelmann, A., 2015. Paleoclimate forcing by the solar De Vries/Suess cycle. *Climate of the Past Discussions*, **11**, 279-305.

Martín-Chivelet, J., Muñoz-García, M.B., Edwards, R.L., Turrero, M.J. and Ortega, A.I., 2011. Land surface temperature changes in Northern Iberia since 4000yr BP, based on $\delta^{13}C$ of speleothems. *Global and Planetary Change*, **77**, 1-12.

McDermott, F., 2004. Palaeo-climate reconstruction from stable isotope variations in speleothems: a review. *Quaternary Science Reviews*, **23**, 901-918.

Meyer, M.C., Faber, R. and Spötl, C., 2006. The WinGeol Lamination Tool: new software for rapid, semi-automated analysis of laminated climate archives. *The Holocene*, **16**, 753-761.

Millán, J.A.A., Gracia, A.G., Tena, M.V.L. and Monterde, J.V.Q., 1992. Parque Cultural de Molinos. Cartografía Temática I. Mapas 1-8, In: *Cartografía Temática I*. (F.B. Mozota and J.I. González, eds.) Publicaciones Parque Cultural de Molinos, Teruel.

Moreno, A., Stoll, H., Jiménez-Sánchez, M., Cacho, I., Valero-Garcés, B., Ito, E. and Edwards, R.L., 2010. A speleothem record of glacial (25–11.6 kyr BP) rapid climatic changes from northern Iberian Peninsula. *Global and Planetary Change*, **71**, 218-231.

Moreno, A., Belmonte, A., Bartolomé, M., Sancho, C., Oliva, B., Stoll, H., Edwards, L.R., Cheng, H. and Hellstrom, J., 2013. Speleothem formation in Northeastern Iberian Peninsula under the influence of different climatic conditions over last glacial cycles. *Cuadernos de Investigación Geográfica*, **39**, 25-47.

Muñoz, A., Sen, A.K., Sancho, C. and Genty, D., 2009. Wavelet analysis of Late Holocene stalagmite records from Ortigosa Caves in Northern Spain. *Journal of Cave and Karst Studies*, **71**, 63-72.

Neff, U., Burns, S.J., Mangini, A., Mudelsee, M., Fleitmann, D. and Matter, A., 2001. Strong coherence between solar variability and the monsoon in Oman between 9 and 6 kyr ago. *Nature*, **411**, 290-293.

Niggemann, S., Mangini, A., Mudelsee, M., Richter, D.K. and Wurth, G., 2003. Sub-Milankovitch climatic cycles in Holocene stalagmites from Sauerland, Germany. *Earth and Planetary Science Letters*, **216**, 539-547.

Peña, J.L., Sánchez-Fabre, M. and Cuadrat, J.M., 2002. *El clima de la provincia de Teruel*. Instituto de Estudios Turolenses. Teruel.

Peña, J.L., Sancho, C., Arenas, A., Auqué, L., Longares, L.A., Lozano, M.V., Meléndez, A., Osácar, C., Pardo, G. and Vázquez-Urbez, M., 2014. Las tobas cuaternarias en el sector aragonés de la Cordillera Ibérica. In: *Las tobas en España* (J.A. González-

Martín and M.J. González-Amuchastegui eds.). *Sociedad Española de Geomorfología,* 159-172.

Peristykh, A.N. and Damon, P.E., 2003. Persistence of the Gleissberg 88-year solar cycle over the last ~12,000 years: Evidence from cosmogenic isotopes. *Journal of Geophysical Research*, **108(A1)**, 1003.

Press, W.H., Teukolsky, S.A., Vetterling, W.T. and Flannery, B.P., 1992. *Numerical Recipes in C*. Cambridge University Press. Cambridge.

Qin, X., Tan, M., Liu, T., Wang, X., Li, T. and Lu, J., 1999. Spectral analysis of a 1000-year stalagmite laminae-thickness record from Shihua Cavern, Beijing, China, and its climatic significance. *The Holocene*, **9**, 689-694.

Raspopov, O.M., Dergachev, V.A., Esper, J., Kozyreva, O.V., Frank, D., Ogurtsov, M. and Shao, X., 2008. The influence of the de Vries (~200-year) solar cycle on climate variations: Results from the Central Asian Mountains and their global link. *Palaeogeography, Palaeoclimatology, Palaeoecology*, **259**, 6-16.

Schimmelmann, A., Lange, C.B. and Meggers, B.J., 2003. Palaeoclimatic and archaeological evidence for a 200-yr recurrence of floods and droughts linking California, Mesoamerica and South America over the past 2000 years. *The Holocene*, **13**, 763-778.

Scholz, D. and Hoffmann, D.L., 2011. StalAge - An algorithm designed for construction of speleothem age models. *Quaternary Geochronology*, **6**, 369-382.

Schulz, M. and Mudelsee, M., 2002. REDFIT: Estimating red-noise spectra directly from unevenly spaced paleoclimatic time series. *Computers and Geosciences*, **28**, 421-426.

Schwabe, A.N., 1844. Sonnen-Beobachtungen im Jahre 1843. *Astron. Nachr*., **21**, 233.

Solanki, S.K., Usoskin, I.G., Kromer, B., Schüssler, M. and Beer, J., 2004. An unusually active Sun during recent decades compared to the previous 11,000 years. *Nature*, **431**, 1084-1087.

Soon, W., Velasco Herrera, V.M., Selvaraj, K., Traversi, R., Usoskin, I., Chen, C.T.A., Lou, J.Y., Kao, S.J., Carter, R.M., Pipin, V., Severi, M. and Becagli, S., 2014. A review of Holocene solar-linked climatic variation on centennial to millennial timescales: Physical processes, interpretative frameworks and a new multiple cross-wavelet transform algorithm. *Earth-Science Reviews*, **134**, 1-15.

Springer, G.S., Rowe, H.D., Hardt, B., Edwards, R.L. and Cheng, H., 2008. Solar forcing of Holocene droughts in a stalagmite record from West Virginia in east-central North America. *Geophysical Research Letters*, **35**, L17703.

Suess, H.E., 1980. The radiocarbon record in tree rings of the last 8000 years. *Radiocarbon*, **22**, 200-209.

Torrence, C. and Compo, G.P., 1998. A practical guide to wavelet analysis. *Bulletin of American Meteorological Society*, **79**, 61-78.

Weedon, G. P., 2003. *Time-Series Analysis and Cyclostratigraphy: Examining Stratigraphic Record of Enviromental Cycles*. Cambridge University Press. Cambridge.

Yu, Z. and Ito, E., 1999. Possible solar forcing of century-scale drought frequency in the northern Great Plains. *Geology*, **27**, 263-266.

Zhang, H.L., Yu, K.F., Zhao, J.X., Feng, Y.X., Lin, Y.S., Zhou, W. and Liu, G.H., 2013. East Asian Summer Monsoon variations in the past 12.5 ka: high-resolution $\delta^{18}O$ record from a precisely dated aragonite stalagmite in Central China. *Journal of Asian Earth Sciences*, **73**, 162-175.

FIGURE CAPTIONS

Figure 1. a) Location and geological setting of Molinos Cave and mean monthly rainfall (mm), maximum and minimum temperature (°C) at the closest meteorological station (Gallipuén reservoir, located 5 km NE of Molinos) averaged over the last five years.

Figure 2. Photograph of the MO-7 stalagmite from Molinos Cave showing the laminated structure. The lines used for the measurement of the colour proxies, and the position of samples used in U/Th dating and stable isotope ($\delta^{18}O$ and $\delta^{13}C$) analysis, are indicated. The figure also includes the 6 continuous-signal records time series of 2170 values (corresponding to R, G, B colour space and CIE L*, a*, b* colour space) with a resolution of 70 microns.

Figure 3. Discrete-signal records time series (4105 data points) of light and dark lamina thickness of the MO-7 stalagmite (a and b). A new time series at annual resolution was derived from the sum of the light and dark values (c).

Figure 4. Discrete-signal records time series (143 data) of isotopic values ($\delta^{18}O$ and $\delta^{13}C$, ‰ PDB) from the MO-7 stalagmite. The sampling interval is 1 mm.

Figure 5. Thin sections of the MO-7 stalagmite. a) General aspect of annual laminae defined by alternating white sparite and dark micrite. b) Columnar calcite with straight boundaries and uniform extinction (crossed polars). Elongated composite calcite crystals are perpendicular to the lamination. c) Laminae of calcite with different thicknesses appear to be grouped into alternating colour bands. Thin lamina ensembles produce dark colours, and thick laminae ensembles produce light colours. d) Thinner laminae are straight, while thicker laminae tend to show a serrated appearance. In this case, peaks reproduce calcite crystal plans.

Figure 6. Age model for the MIS 1 interval of the MO-7 stalagmite. a) A 1:1 slope that allows to identify the hiatus in the stalagmite, b) Laminae age model after anchoring to U/Th ages, c) Final age-model (StalAge) used for the different proxies.

Figure 7. Lamina thickness (a); colour proxies (R, G, B, L*,a* and b*) (b to g) and U/Th dates with error bars (depth from top) next to the 4.3-4.9-kyr hiatus (h) in the MO-7 stalagmite. Lamina thickness with a smoothing window of 100 years and colour records smoothed with a 15-point moving average. Note the inverse axes for the a* and b* colour proxies.

Figure 8. Fourier spectral analysis for unevenly sampled data from the Holocene interval of the MO-7 stalagmite (4 time series R, G, B and L* colour parameters,

comprising 2170 data with an interval sample of 70 m□□□□□□). (a) Spectra estimated with the Lomb periodogram algorithm that determines the 0.01 and 0.05 significance levels (white noise lines) of the colour time series. The spectra show well defined periodicities at 91-yr (Gleissberg cycle), 170-yr (De Vries-Suess cycle) and 421-yr. (b) Spectra estimated using the REDFIT program (3 segments with 30% overlap). The spectral window is rectangular. The time series is compared with an AR(1) red noise model. The maxima in the spectral power have a less than 1% chance of being part of the AR(1) red noise model. The spectra show a well-defined periodicity at 91 years (Gleissberg cycle).

Figure 9. Wavelet analysis of the lamina couplet thickness time series (wavelets with a white-noise model and a Morlet window at 95% significance level, red noise model). The black dashed contour defines the periodicities within the 95% confidence level, and the continuous black line defines the cone of significance. The spectra from the lower and upper sections show the same periodicities (Gleissberg and De Vries-Suess cycles and a lower-frequency cycle of approximately 400 years). In the lower section of the stalagmite, all these cycles are well defined. The Gleissberg cycle is discontinuous but is well represented in the interval 7.2-6.5 kyr. In the upper section, both the Gleissberg and De Vries-Suess cycles are discontinuous; the Gleissberg is well represented in the range 3.6-2.5 kyr whereas the De Vries-Suess is better defined in the interval 4.3-3.2 kyr.

Figure 10. Fourier spectral analysis of 2 time series of 143 data derived from the isotopic values ($\delta^{18}O$ and $\delta^{13}C$) of the MO-7 stalagmite (1 segment without overlap). The spectral window is rectangular. The time series is compared with an AR(1) red noise model. The maxima in spectral power have a less than 5% chance

of being part of the AR(1) red noise model. The spectra show a periodicity of 183 years, roughly corresponding to the De Vries-Suess cycle.

Figure 11. Correlation panel for the MO-7stalagmite. a) $\delta^{18}O$ record from the North Greenland Ice Core Projet (5-point moving average), b) % hematite stained grain (Bond et al., 2001), c) L* parameter (17-point moving average), d) laminae thinckness (53-point moving average), e) and f) $\delta^{13}C$ and $\delta^{18}O$ record from MO-7 stalagmite, respectively, g) MO-7 U/Th ages, h) sunspot number (11-point moving average) from Solanki et al. (2004). In all cases, the climate interpretation is on the y-axis.

Table 1. U-Th activity ratios and calculated ages. Activity ratios were determined by MC-ICP-MS following Hellstrom (2003). Ages in kyr before present were corrected for the initial ^{230}Th concentration using Eqn. 1 of Hellstrom (2006), ($^{230}Th/^{232}Th$)i of 0.9±0.6 and the decay constants of Cheng et al (2013). Uncertainties were propagated using Monte Carlo simulations of each of the input activity ratios. The initial ($^{234}U/^{238}U$) was calculated using the corrected age of each sample. U content is marked as “n.r.” where sample weights were not recorded.

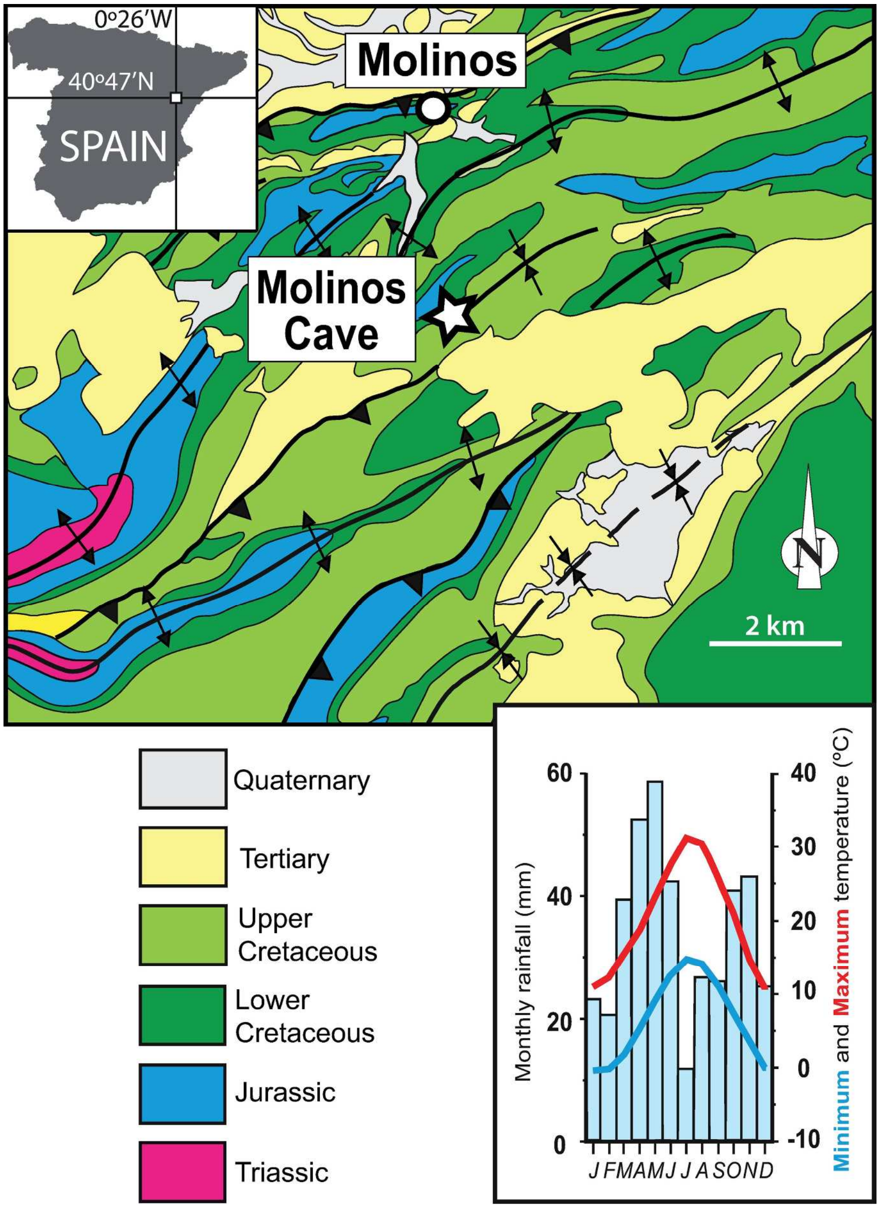

Location of the study area
199x274mm (300 x 300 DPI)

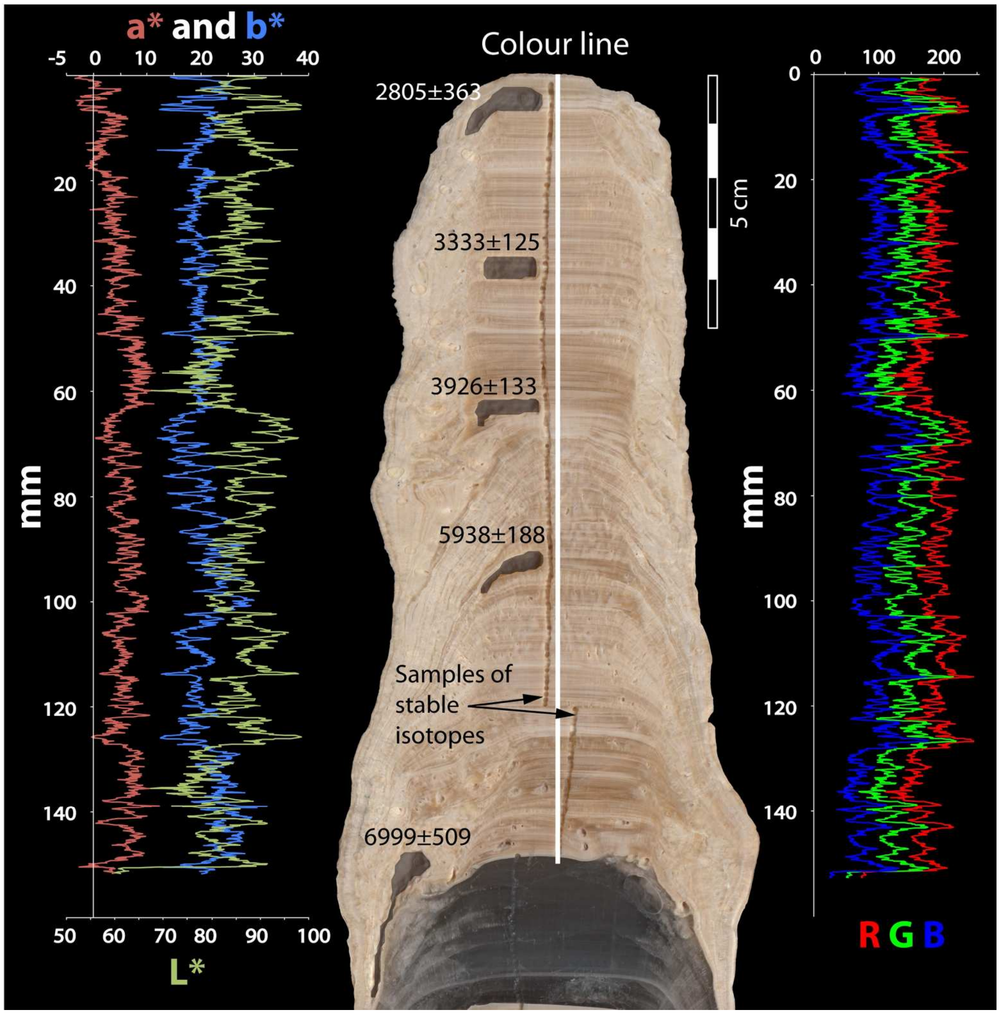

MO-7 stalagmite
196x199mm (300 x 300 DPI)

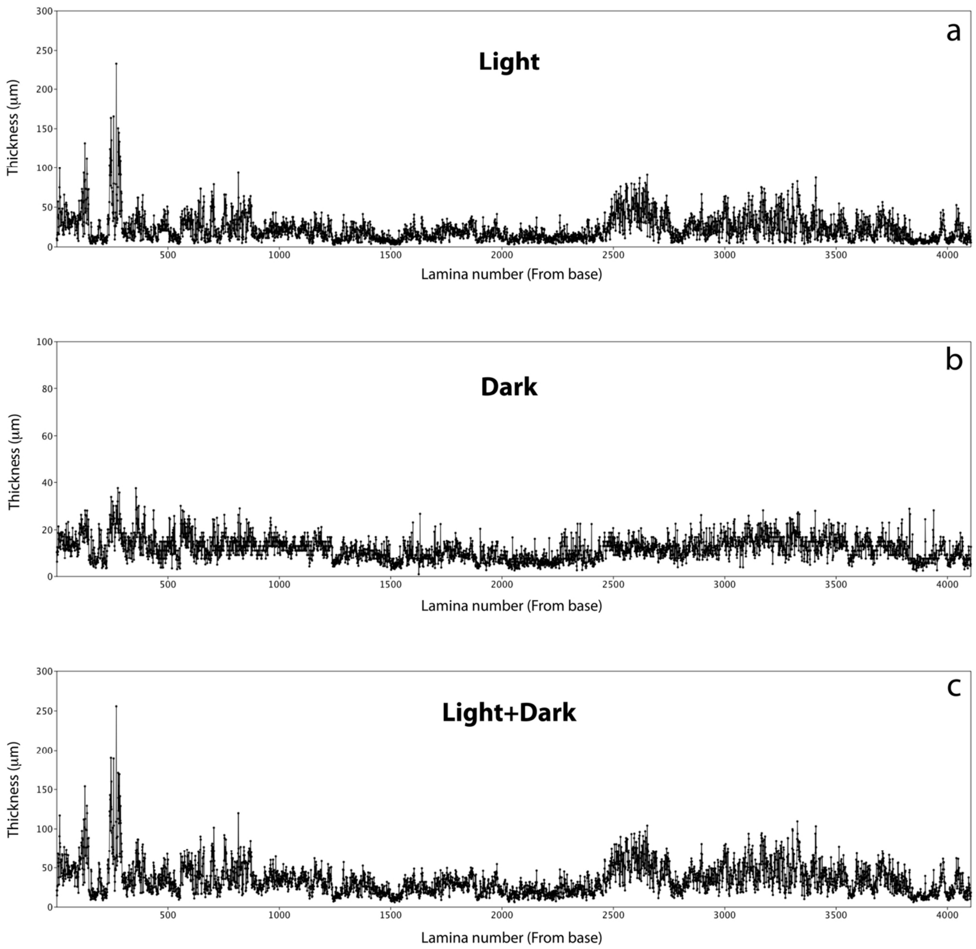

Thickness
175x170mm (300 x 300 DPI)

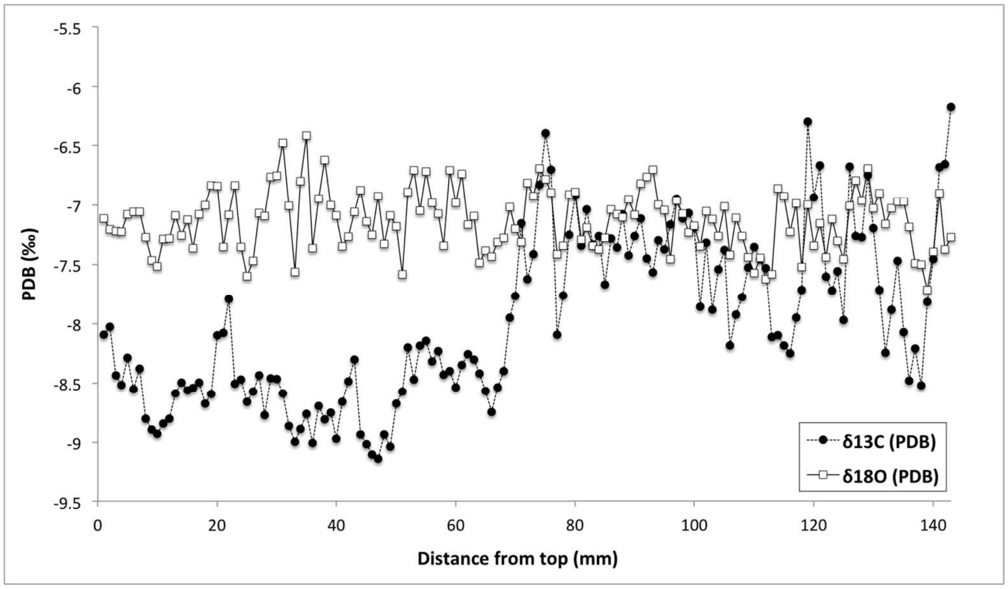

Isotopes
162x94mm (300 x 300 DPI)

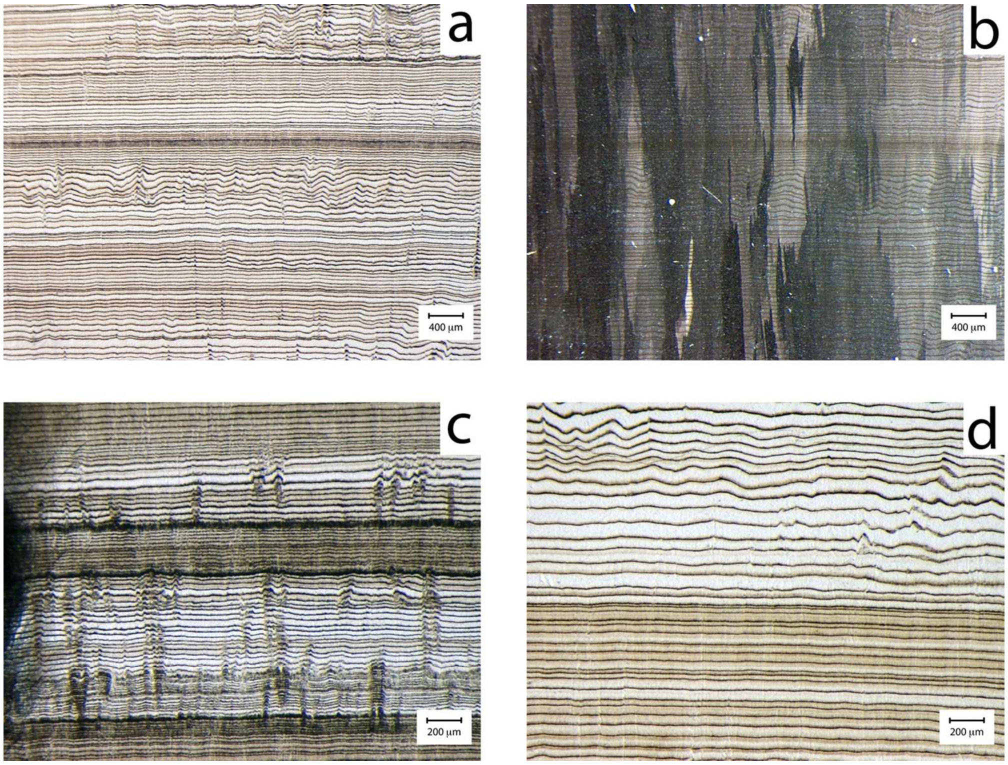

Lamination
136x102mm (300 x 300 DPI)

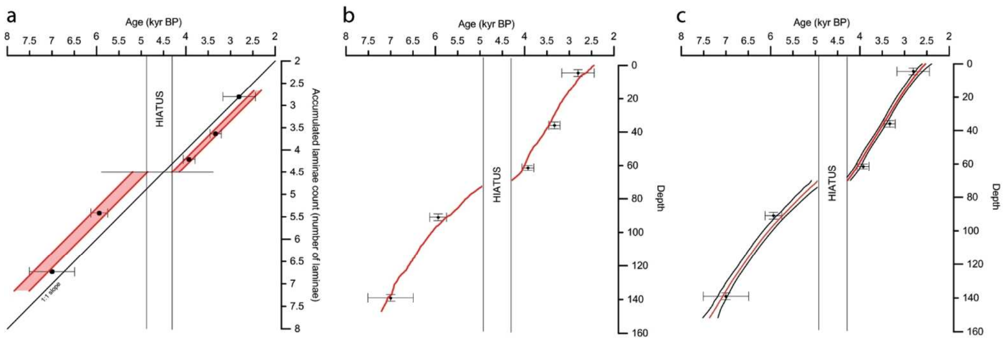

Age model
192x64mm (300 x 300 DPI)

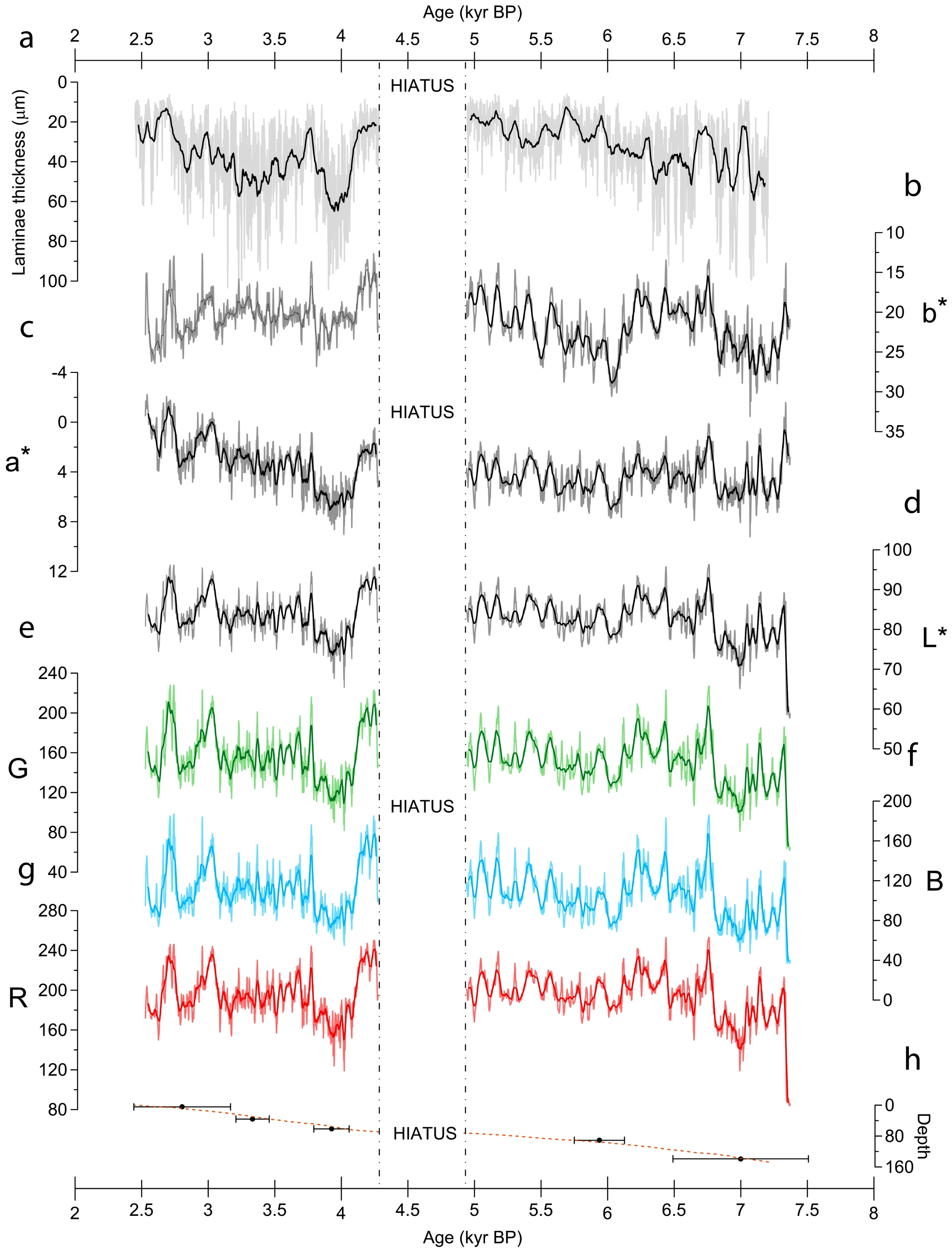

Time series
728x961mm (600 x 600 DPI)

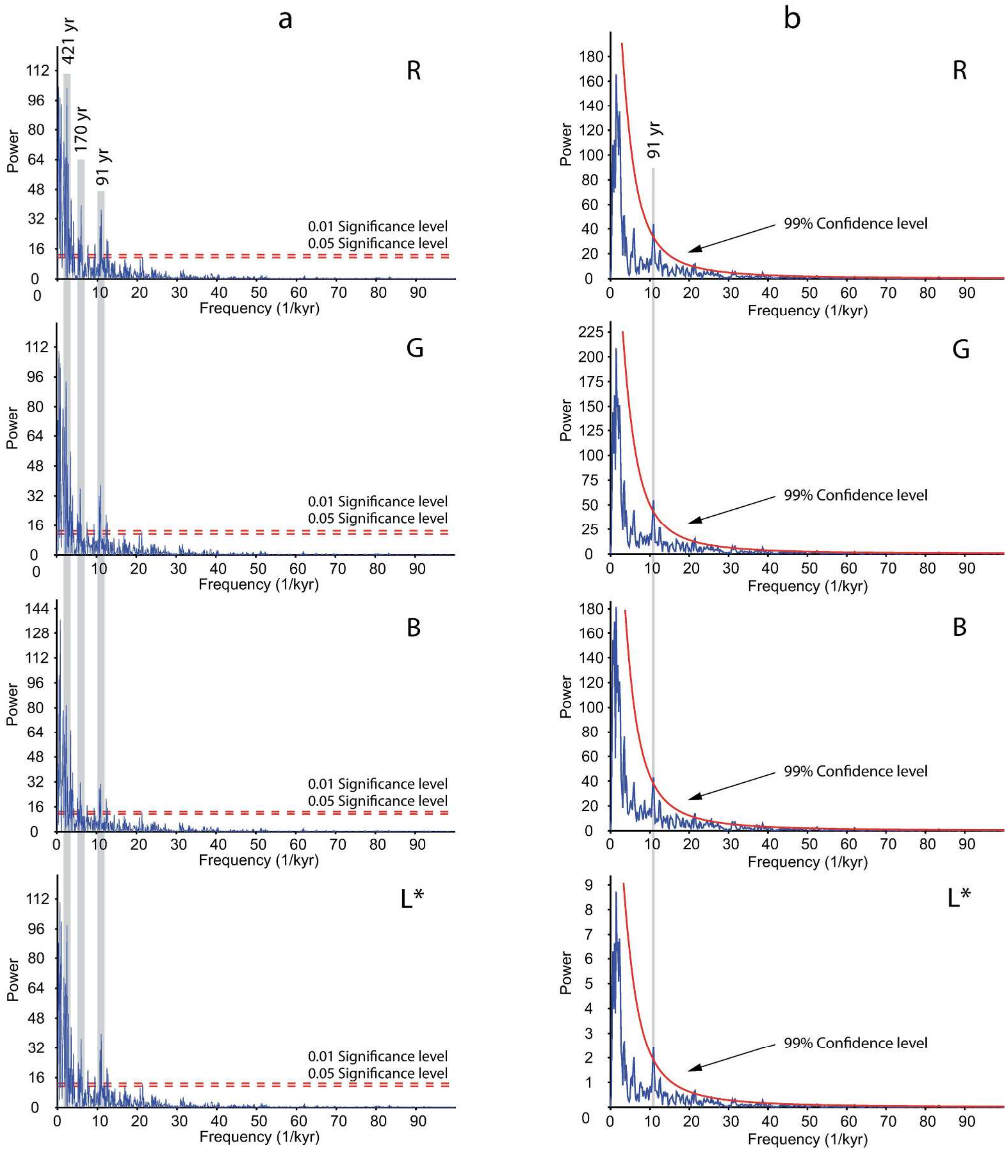

Fourier spectra
264x303mm (300 x 300 DPI)

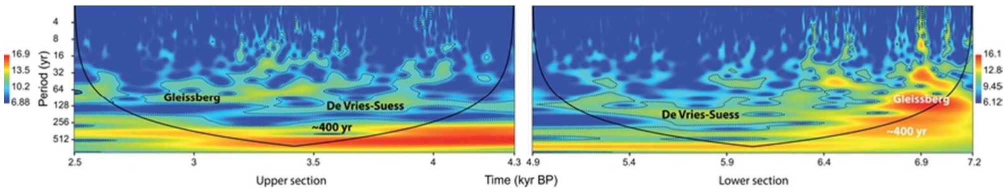

Wavelet
74x13mm (300 x 300 DPI)

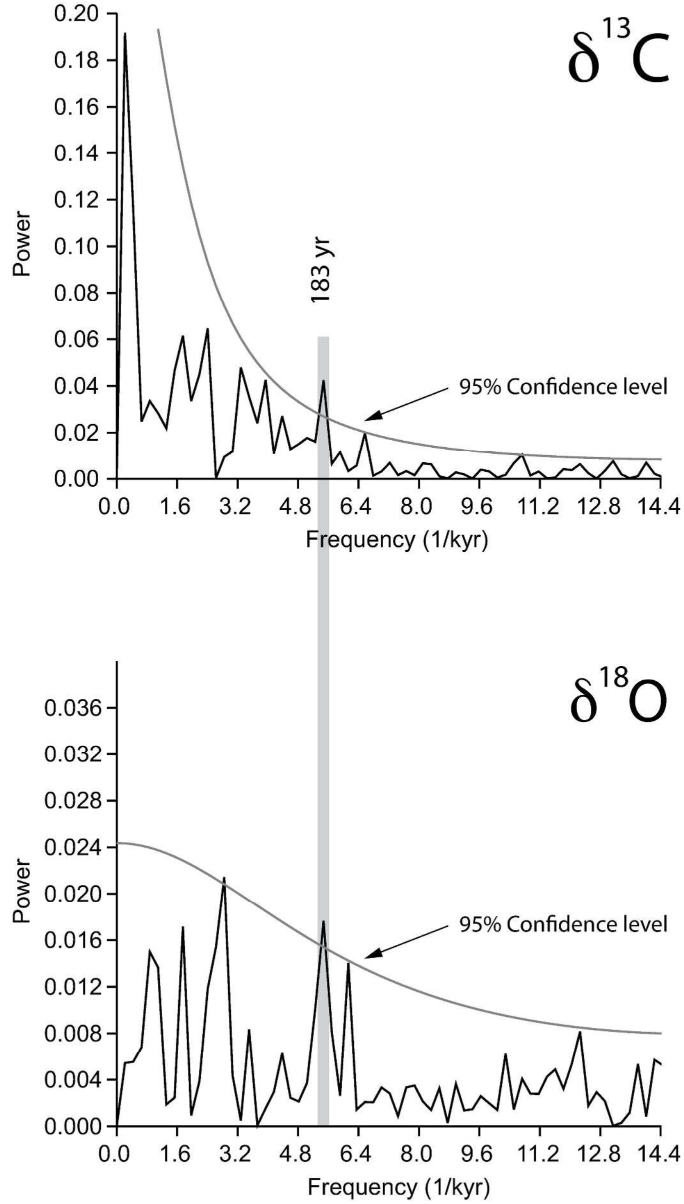

Fourier-isotopes
217x376mm (300 x 300 DPI)

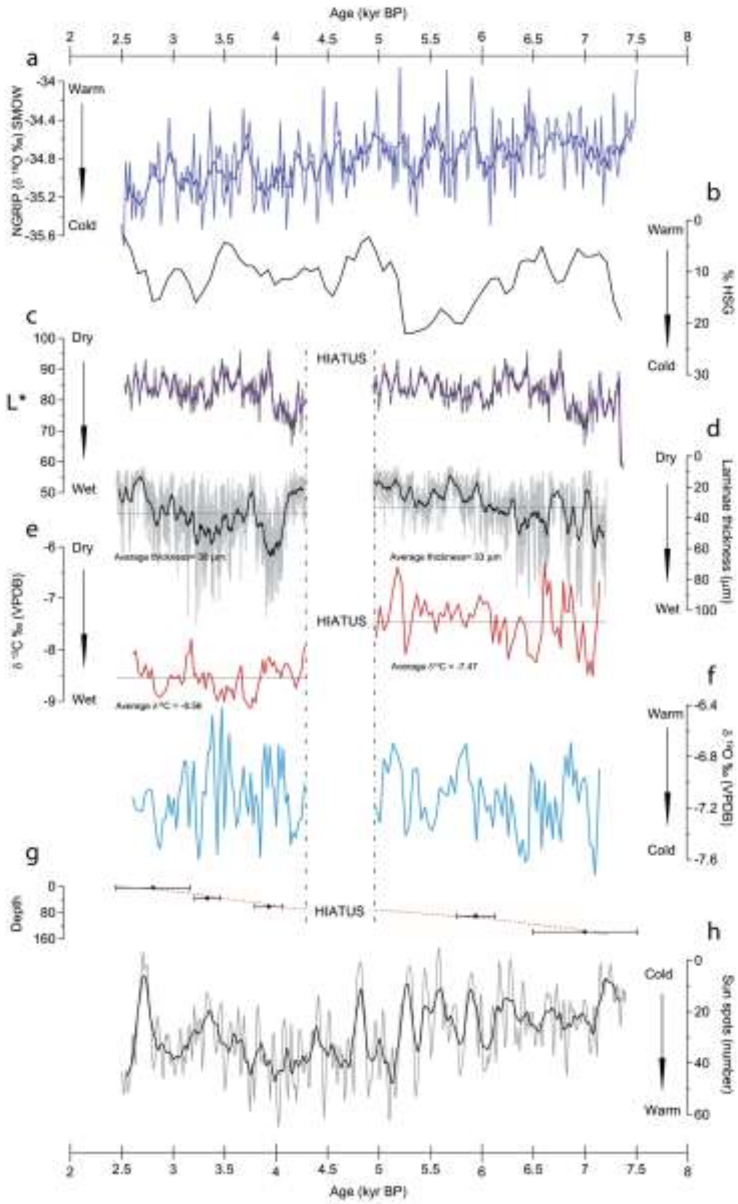

Correlation
730x1196mm (600 x 600 DPI)

Sample and depth	Laboratory ID	U(ngg-1)	(230Th/238U)	(234U/238U)	(232Th/238U)	(230Th/232Th)	Age(ka)	(234U/238U)i
MO-7 4.5 mm	UMB03451 Sep-2010	n.r.	0.0301(13)	1.0118(37)	0.00502(18)	6.0	2.81(.36)	1.0119(37)
MO-7 36 mm	UMB03905 Feb-2011	80	0.0313(08)	1.0015(30)	0.00131(02)	23.8	3.33(.13)	1.0015(30)
MO-7 61.5 mm	UMB03904 Feb-2011	70	0.0364(08)	0.9935(30)	0.00146(01)	24.9	3.93(.13)	0.9934(31)
MO-7 91 mm	UMB03901 Feb-2011	64	0.0536(14)	0.9889(34)	0.00141(04)	38.2	5.94(.19)	0.9887(35)
MO-7 139 mm	UMB03450 Sep-2010	n.r.	0.0653(25)	0.9688(47)	0.00602(21)	10.9	7.00(.51)	0.9682(47)